Investigation of Temperature History, Porosity and Fracture Mode on AA1100 Using the Controlled Intermittent Wire Feeder Method

Baskoro, Sunar, Ario
Department of Mechanical Engineering, Faculty of Engineering, Universitas Indonesia

Amat, Azwar, Mohammad
Department of Mechanical Engineering, Faculty of Engineering, Universitas Indonesia

Putra, Dwi, Rahadian
Department of Mechanical Engineering, Faculty of Engineering, Universitas Indonesia

Widyianto, Agus
Department of Mechanical Engineering, Faculty of Engineering, Universitas Indonesia

他

https://doi.org/10.5109/2740953

出版情報：Evergreen. 7 (1), pp.86-91, 2020-03. 九州大学グリーンテクノロジー研究教育センター
バージョン：

Investigation of Temperature History, Porosity and Fracture Mode on AA1100 Using the Controlled Intermittent Wire Feeder Method

Ario Sunar Baskoro[1,*], Mohammad Azwar Amat[1], Rahadian Dwi Putra[1], Agus Widyianto[1], Yala Abrara[1]

[1]Department of Mechanical Engineering, Faculty of Engineering, Universitas Indonesia, Kampus UI Depok 16424, Indonesia

*Ario Sunar Baskoro,
E-mail: ario@eng.ui.ac.id

(Received October 31, 2019; Revised December 16, 2019; accepted February 24, 2020).

Abstract: In this study, the effect of variation of intermittent wire feeding method on thermal histories during the welding process, the physical appearance, mechanical properties, and fracture mode was investigated. The configuration parameter of wire feeding was determined by the properties of the so-called length ratio (RL). It was influenced by welding speed, wire feeding speed, feeding time, and delaying time. Bigger value of length ratio tends to have a smaller bead width with a higher cap. Also, a larger ratio tends to have bigger tensile strength and the fracture location close to the weld bead.

Keywords: GTAW; ratio filler; intermittent wire filler; temperature; fracture

1. Introduction

Aluminum alloys are well known and one of the most important materials in the world. It is found in wide range applications such as aerospace industries, railway vehicles, high-speed ships, most window panels, light structures, heavy structures, offshores structures, and bridges[1-4]. Aluminum alloys also have good corrosion resistance and strength to weight ratio[5-8]. There are many variants to joint aluminum, such as RSW[9, 10], FSW/FSSW[11, 12], GMAW[13, 14], one of the most widely joint processes for aluminum alloys is GTAW, it utilizes an inert gas for arc shielding and non-consumable tungsten (pure or alloy) electrode[15, 16]. GTAW process has several advantages such as stable process, high quality with less spatter, and good weld bead appearance. However, GTAW has some disadvantages, such as incomplete fusion, hot cracking, porosity, lack of deposition, and reduced strength in HAZ region[17-19]. Automatic wire feeding in TIG welding is similar to the method in MIG welding. However, it has two separate mechanisms that need to be synchronized with each other to get a good result of the weld.

There are aluminum alloy series that are often used, such as the AA1xxx series and AA6xxx series[20]. The aluminum series has advantages such as good weldability, resistance to corrosion, easy to form, and relatively lower cost[21]. Aluminum alloy AA1100 series has several properties such as high thermal conductivity, high machinability, corrosion resistance, and light in weight[22]. Aluminum alloys can also be heat treated to precondition for aging and improve phase structure without precipitation[23].

The intermittent wire feeding method has been described by Ario et al.[24] in elsewhere paper, the configuration parameter was influenced by welding speed, wire feeding speed, feeding time, and delaying time. Figure 1 shows pulsation timing feeding (ON) and delaying (OFF) in 1 cycle time period. In the previous work of Ario et al. (2019), the preliminary investigation of the intermittent wire feeding method has been developed using AA6063 and ER5356 as the base metal and filler metal. They investigated physical appearance, macrostructure, and microstructure on the weld metal. Maurya[25] reported the use of Al 6061 to be made into metal matrix composites with SiC particle variations. In other research, Milyardi[26] investigated the influence of speed and current in autogenous GTAW of AA1100 on porosity. They reported that the welding speed had a significant effect on porosity. The EDS study revealed that the localized segregation occurs on the center WM with the high-density second phase. The Mg content from the filler metal was concentrated in the area where filler metal was inserted, also the fast cooling rates while the filler was inserted made the localized region more columnar structured with boundaries outside. The author also proposes a method to calculate the length ratio and volume ratio. Regarding the previous work, the exploration of different scale of length ratio (RL) was investigated in this

study. This paper aims to investigate the effect of different RL on thermal histories, physical appearance, porosity, and mechanical properties.

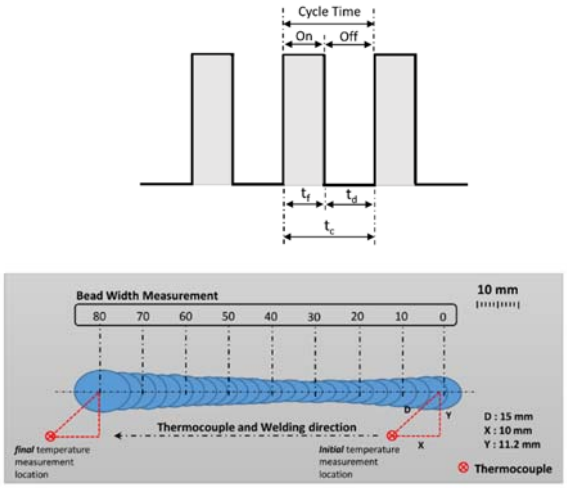

Fig. 1: Cycle time, feeding time and delaying time schematic illustration (top), thermocouple arrangement and bead width measurement (bottom)

2. Method

AA1100 with a thickness of 3 mm and ER1100 with a diameter of 1.2 mm was used as base metal and filler metal. The specimen was cut into 120 x 50 x 3 mm, a butt joint configuration was prepared for the GTAW joint. The mechanical property of base metal AA1100 was 130 MPa. Welding length was set 80 mm with 2 mm/s welding speed and 10 second pre-heating time. The specimens were clamped to avoid distortion, and the thermocouple was set, as shown in Figure 1. High purity argon (99.9%) with 9 L/min of flow rate was applied. An AWS class EWTH-2 tungsten electrode with a diameter of 2.4 mm was used. The welding parameter was set on AC mode with a frequency of 50 Hz and a current 160A on all configurations. The length ratio configuration parameter is shown in Table 1. Weld bead measurement was carried out using Dino Lite as shown in Figure 1. Porosity observation was carried out by X-Ray Radiograph Rigaku RF-300EGM2. ASME standard has been used with the distance of shooting range 1200 mm, flashing time 15 s, with 400 mA current. Tensilon RTF-2350 universal testing machine 50 kN was used to carry out tensile testing.

Table 1. Length ratio parameter design of experiment

Ratio	Welding speed (mm/s)	Wire feeder speed (mm/s)	Feeding time (s)	Delay time (s)	Filler debit (m^3/s)
1	2	8	0.25	0.75	2.26
2	2	8	0.5	0.5	4.52
3	2	8	0.75	0.25	6.79
4	2	16	0.5	0.5	9.05
5	2	16	0.625	0.375	11.31
6	2	16	0.75	0.25	13.57

3. Results

As shown in Figure 2, temperature histories of the HAZ region show the pre-heating temperature reached 90 – 110°C within 10 s and reached peak temperature 260 – 300°C in the final section after 50 s welding process. The ratio has not straight correlation through the temperature history in the HAZ region. Figure 3 shows the top bead, back bead, and porosity appearance on all ratio configuration. Larger ratio equals to more filler, resulted in a higher cap, smaller bead width, and higher tendency to show large pores. Figure 3(a,b) show ratio 1 and 2, and there was no porosity occurred in the weldment. Figure 3(c) shows large porosity appeared on ratio 3 as a result of too low the welding temperature process (As shown in Figure 2). Figure 3(d,e) show the result of ratio 4 and 5, porosity becomes less dense compared to ratio 3, because the welding temperature was higher compared to ratio 3. Figure 3(f) shows large and dense porosity occurred in the ratio 6.

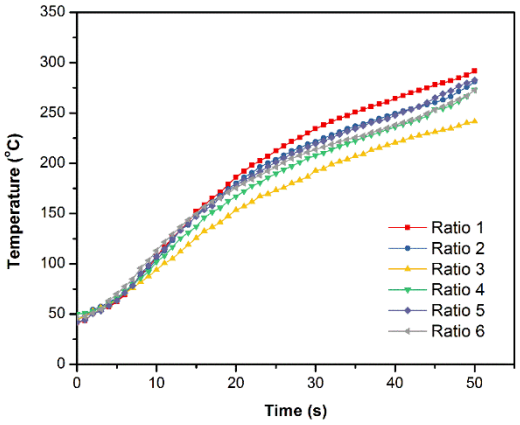

Fig. 2: Temperature histories at HAZ region

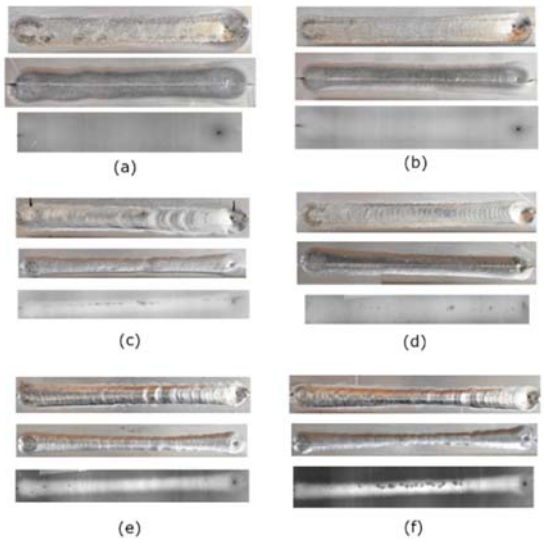

Fig. 3: Physical appearance at top and back position and X-ray image (a) ratio 1, (b) ratio 2, (c) ratio 3, (d) ratio 4, (e) ratio 5, and (f) ratio 6

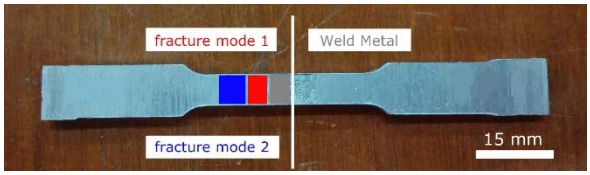

Fig. 4: Tensile specimen shape with characterized fracture based on location

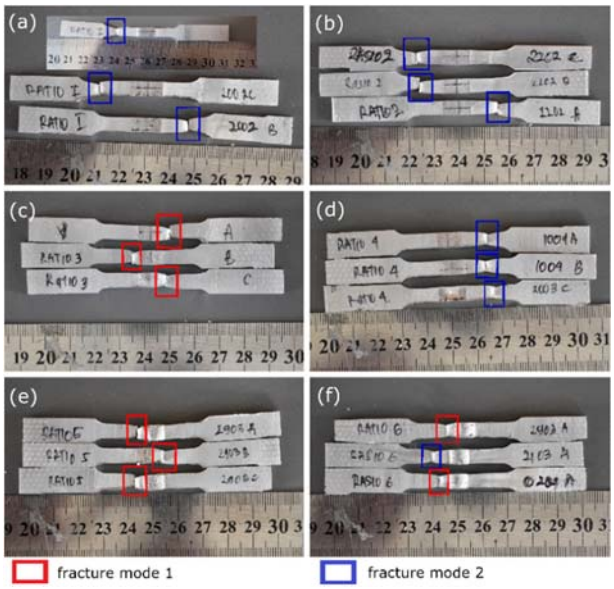

Fig. 5: All specimens fracture spot

Figure 4 shows a tensile specimen and fracture characterized based on the location of the fracture. Fracture mode 1 shows in the red area, and fracture mode 2 shows in a blue area, the grey area shows the weld metal region. Figure 5 shows all fracture specimens and the fracture mode. Figure 6(a-c) show the result of tensile testing on all specimens. The result shows a straight correlation between fracture location and tensile strength. Fracture mode 1 has higher tensile strength and shorter strain, and fracture location took place between 2 – 7 mm from weld lines, it is not completely annealed or half annealed. Fracture mode 2 has lower tensile strength and longer strain, and fracture location took place between 9 – 15 mm, it is completely annealed or fully annealed. Figure 7(d) shows the average of UTS vs. Length Ratio (RL). Fracture mode 1 shows tensile strength between 70 – 76 MPa with an average of 74 MPa, while fracture mode 2 shows tensile strength between 76 – 93 MPa with an average of 86 MPa. Figure 7 shows the U-shape of the top bead width and back bead width. Figure 7(a) shows that 9 mm in size is the boundary of the top bead width (TBW) between fracture mode 1 and fracture mode 2. While Figure 7(b) shows that 8 mm in size is the boundary of the back bead width (BBW) between fracture mode 1 and fracture mode 2.

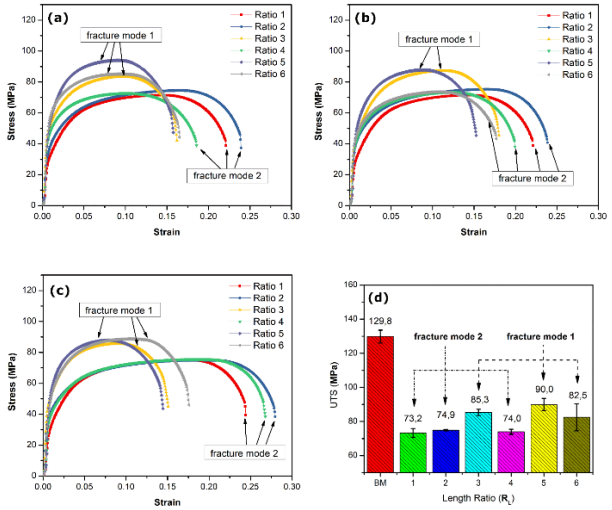

Fig. 6: Result of tensile test (a) sample 1, (b) sample 2, (c) sample 3, and (d) average ultimate tensile strength (UTS)

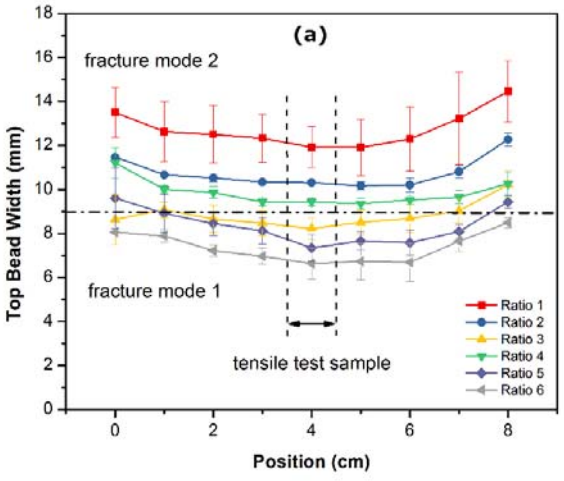

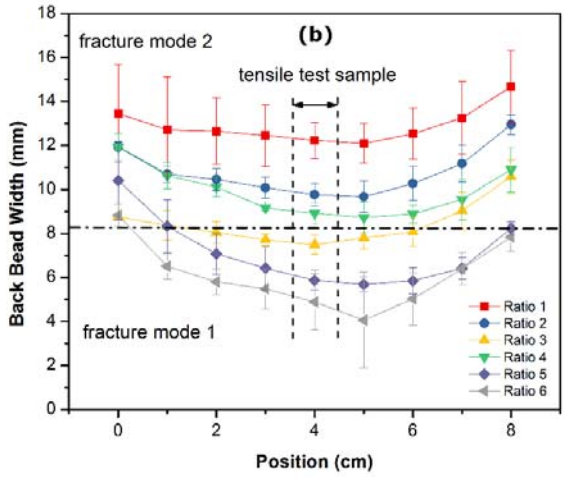

Fig. 7: Result of measurement (a) Top bead width and (b) Back bead width

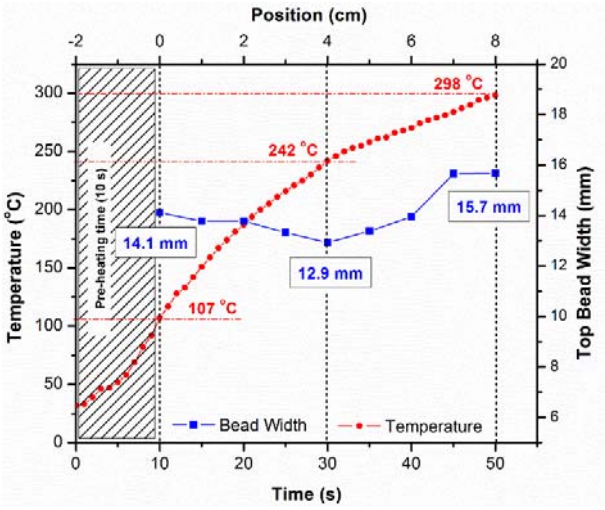

Fig. 8: Temperature history vs. Top bead width plotting scheme (ratio 1, sample 1)

Figure 8 shows the schematic plot temperature vs. TBW. The plotting location were 0, 4, and 8 cm then matched with the temperature history. At the 0 cm location, the top bead width was 14.1 mm, and the temperature was 107°C. At the 4 cm location, the top bead width was 12.9 mm, and the temperature was 242°C. At 8 cm location, the top bead width was 15.7 mm, and the temperature was 298°C.

Figure 9 shows plotting temperature and TBW on all ratio configuration (a) at 0 cm location, (b) at 4 cm location, and (c) at 8 cm location. The result shows TBW tends to decrease with an increase in length ratio.

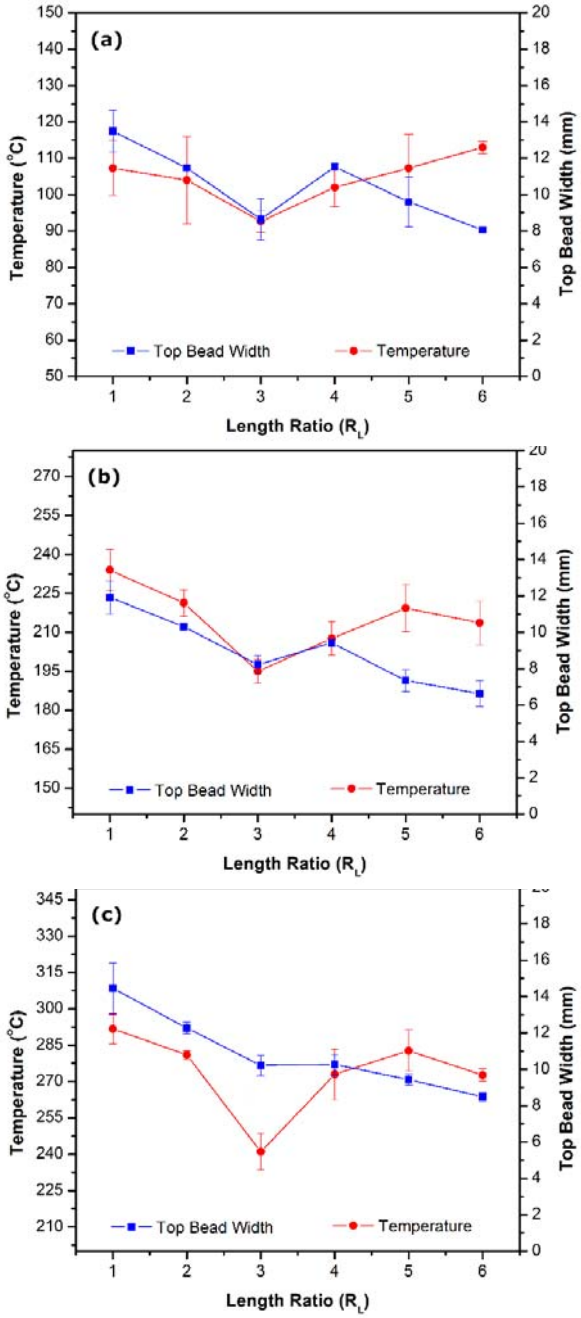

Fig. 9: Temperature vs. Top bead width on all ratio (a) at location 0 cm, (b) 4 cm, and (c) 8 cm

4. Conclusions

In general, increasing length ratio (hence, increasing volume of filler) would decrease TBW and BBW, increase large porosity to occurs, tendency to have higher tensile strength and potential to fracture at mode 1. In general, more heat input would make it more time to grow up a new grain formation. This result was similar to Liang et al.[27], the more heat added in the welding process, more far away the softened zone from the center of the weld. And it made the tensile strength reduced even more. There is no distinct correlation between temperature histories at

the HAZ region and length ratio. However, the result of ratio 3 suggests that the drop in temperature while performing the welding process would result in decreasing the size of TBW and BBW, increasing the tendency to large porosity occurs and potential to fracture mode 1.

Acknowledgements

This research is supported by PITTA B Research Grant in 2019 program of Directorate of Research and Public Services, Universitas Indonesia with contract number NKB-0706/UN2.R3.1/HKP.05.00/2019.

References

1) A. S. Baskoro, A. Fauzian, H. Basalamah, G. Kiswanto, W. Winarto, Improving weld penetration by employing of magnetic poles' configurations to an autogenous tungsten inert gas (TIG) welding, *The International Journal of Advanced Manufacturing Technology*, **99**, 1603-1613 (2018).
2) R. Manti, D. Dwivedi, A. Agarwal, Microstructure and hardness of Al-Mg-Si weldments produced by pulse GTA welding, *The International Journal of Advanced Manufacturing Technology*, **36**, 263-269 (2008).
3) N. Mohd, M. M. Kamra, M. Sueyoshi, C. Hu, Three-dimensional Free Surface Flows Modeled by Lattice Boltzmann Method: A Comparison with Experimental Data, *Evergreen: joint journal of Novel Carbon Resource Sciences & Green Asia Strategy*, **4**, 29-35 (2017).
4) H. Li, J. Zou, J. Yao, H. Peng, The effect of TIG welding techniques on microstructure, properties and porosity of the welded joint of 2219 aluminum alloy, *Journal of Alloys and Compounds*, **727**, 531-539 (2017).
5) M. Imam, V. Racherla, K. Biswas, Design, Effect of post-weld natural aging on mechanical and microstructural properties of friction stir welded 6063-T4 aluminium alloy, *Materials & Design*, **64**, 675-686 (2014).
6) Y. Huang, D. Wu, N. Lv, H. Chen, S. Chen, Investigation of porosity in pulsed GTAW of aluminum alloys based on spectral and X-ray image analyses, *Journal of Materials Processing Technology*, **243**, 365-373 (2017).
7) A. Lakshminarayanan, V. Balasubramanian, K. Elangovan, Effect of welding processes on tensile properties of AA6061 aluminium alloy joints, *The International Journal of Advanced Manufacturing Technology*, **40**, 286-296 (2009).
8) C. Zhang, M. Gao, D. Wang, J. Yin, X. Zeng, Relationship between pool characteristic and weld porosity in laser arc hybrid welding of AA6082 aluminum alloy, *Journal of Materials Processing Technology*, **240**, 217-222 (2017).
9) M. F. Arifardi, A. S. Baskoro, M. A. Amat. Development of 2-dimensional finite element modeling of resistance spot welding: 1st generation model electric-thermal coupled. AIP Publishing.
10) A. S. Baskoro, H. Muzakki, G. Kiswanto, W. Winarto, Mechanical Properties and Microstructures on Dissimilar Metal Joints of Stainless Steel 301 and Aluminum Alloy 1100 by Micro-Resistance Spot Welding, *Transactions of the Indian Institute of Metals*, **72**, 487-500 (2019).
11) Suwarsono, Budiono, A. S. Baskoro, G. Kiswanto. Mechanical properties of friction stir lap welding (FSLW) on dissimilar aluminum sheet A1100 and A1050. AIP Publishing.
12) R. Acuña, C. M. Abreu, M. J. Cristóbal, M. Cabeza, X. R. Nóvoa, Electrochemical study of the surface metal matrix composite developed on AA 2024-T351 by the friction stir process, *Corrosion Engineering, Science and Technology*, **54**, 715-725 (2019).
13) R. Ahmad,M. A. Bakar, Effect of a post-weld heat treatment on the mechanical and microstructure properties of AA6061 joints welded by the gas metal arc welding cold metal transfer method, *Materials & Design*, **32**, 5120-5126 (2011).
14) P. Luchtenberg, P. T. de Campos, P. Soares, C. A. H. Laurindo, O. Maranho, R. D. Torres, Effect of welding energy on the corrosion and tribological properties of duplex stainless steel weld overlay deposited by GMAW/CMT process, *Surface and Coatings Technology*, **375**, 688-693 (2019).
15) Y. Tarng,W. Yang, Optimisation of the weld bead geometry in gas tungsten arc welding by the Taguchi method, *International Journal of Advanced Manufacturing Technology*, **14**, 549-554 (1998).
16) K. R. Ramkumar,S. Natarajan, Optimization of GTAW Al 3003 weld using fabricated nanocomposite filler metal, *Materials and Manufacturing Processes*, **34**, 293-302 (2019).
17) Y. Liang, S. Hu, J. Shen, H. Zhang, P. Wang, Geometrical and microstructural characteristics of the TIG-CMT hybrid welding in 6061 aluminum alloy cladding, *Journal of Materials Processing Technology*, **239**, 18-30 (2017).
18) R. Manti,D. K. Dwivedi, Microstructure of Al–Mg–Si weld joints produced by pulse TIG welding, *Materials and Manufacturing Processes*, **22**, 57-61 (2007).
19) K. Zhang, J. Chen, P. Ma, X. Zhang, Effect of welding thermal cycle on microstructural evolution of Al–Zn–Mg–Cu alloy, *Materials Science and Engineering A*, **717**, 85-94 (2018).
20) Z. Aminah, S. Noraini, H. Zuhailawati, A. Anasyida. Effect of solution treatment on Al 1100 cryorolled sheet alloy. in *IOP Conference Series: Materials Science and Engineering*. 2016. IOP Publishing.
21) H.-l. Yu, A. K. Tieu, C. Lu, X.-h. Liu, A. Godbole, C. Kong, Mechanical properties of Al–Mg–Si alloy

sheets produced using asymmetric cryorolling and ageing treatment, *Materials Science and Engineering: A*, **568**, 212-218 (2013).
22) P. Kumar, P. G. Scholar, S. Katiyar, Effect of Mechanical Mould Vibration on the Properties of Sand Casting Aluminium (A-1100) Alloy.
23) V. M. Monteiro, S. B. Diniz, B. G. Meirelles, L. C. Da Silva, A. d. S. Paula, Microstructural and Mechanical study of aluminium alloys submitted to distinct soaking times during solution heat treatment, *Tecnologia em Metalurgia, Materiais e Mineração*, **11**, 332 (2014).
24) A. S. Baskoro, M. A. Amat, A. I. Pratama, G. Kiswanto, Winarto, Effect of tungsten inert gas (TIG) welding parameters on macrostructure, microstructure and mechanical properties of AA6063-T5 using the controlled intermittent wire feeding method, *International Journal of Advanced Manufacturing Technology*, (2019). (**Article in Press**)
25) M. Maurya, N. K. Maurya, V. Bajpai, Effect of SiC Reinforced Particle Parameters in the Development of Aluminium Based Metal Matrix Composite, *Evergreen*, **6**, 200-206 (2019).
26) I. Milyardi,A. S. Baskoro. Effect of current and speed on porosity in autogenous Tungsten Inert Gas (TIG) welding of aluminum alloys A1100 butt joint. IOP Publishing.
27) Y. Liang, J. Shen, S. Hu, H. Wang, J. Pang, Effect of TIG current on microstructural and mechanical properties of 6061-T6 aluminium alloy joints by TIG–CMT hybrid welding, *Journal of Materials Processing Technology*, **255**, 161-174 (2018).